Deflection of non-Newtonian simple shear flow around a rigid cylindrical body by the Finite Element Method

TOSHIAKI MASUDA and NAOYA MIZUNO*

Institute of Geosciences, Shizuoka University, Shizuoka 422, Japan

Abstract—This paper describes flow during simple shear of non-Newtonian (power-law) viscous materials around a rigid cylindrical body, and examines how the magnitude of the stress exponent (n) influences the deflection of particle paths as well as dynamic and kinematic quantities. A limited range of values (1–5) of n was used in the analysis. The angular velocity of the cylinder is half of the far-field shear strain rate, which is exactly the same as that for a Newtonian fluid. Particle paths always exhibit a 'double-bulge shaped' separatrix, the size of which slightly decreases with increasing n. The maximum values of pressure and differential stress also slightly decrease while that of vorticity and kinematic vorticity number increase as n increases, although the maximum change is less than 24% from $n = 1$ to $n = 5$. The general pattern of distribution of these dynamic and kinematic quantities around the cylinder for different values of n look similar. The non-Newtonian flows are, as a first approximation, similar to the Newtonian one. Copyright © 1996 Elsevier Science Ltd

INTRODUCTION

The experimental deformation of rock at high temperature and pressure has revealed that the relationship between compressional strain rate ($\dot{\varepsilon}$) and differential stress (σ) during steady-state flow is well represented by the power-law equation, $\dot{\varepsilon} = A \sigma^n \exp(-Q/RT)$, where A is the material constant, R is the gas constant, T is the absolute temperature, Q is the activation energy for creep, and n is the stress exponent (e.g. Nicolas & Poirier 1976, Poirier 1985). A wide range of values of A, n and Q for different rock types or minerals has been proposed. In this paper we investigate the stress exponent n. For most minerals and rocks, n has a value between 2 and 7 (e.g. Carter & Tsenn 1987, Kirby & McCormick 1989). Theoretical studies have demonstrated that various mechanisms affect the value of n (e.g. Nicolas & Poirier 1976, Poirier 1985). Recently, Wang *et al.* (1994) demonstrated the importance of Harper-Dorn creep ($n = 1$) in the deep crust and the mantle, and discussed how greatly stress estimates are influenced by the magnitude of n: the stress estimate differs by several orders of magnitude between $n = 1$ and $n = 3$. Thus, n is one of the most important variables in the quantitative evaluation of stress levels in the crust and mantle.

At present, we have at least three ways of inferring the magnitude of n during natural deformation. The first involves deformation mechanism analysis, and uses dislocation substructures as keys to bridge experimental and theoretical analyses and natural samples. Dislocation substructures in most mylonites suggest that n is 3 during mylonitization. This method principally depends on extrapolation of the experimental results to natural conditions.

The second method involves fold shape analysis. Hudleston & Lan (1994) showed that fold shape is highly influenced by n and tried to estimate n of siltstone layers by comparing shapes of theoretical and natural folds. The third way utilises the shape of mantled porphyroclasts in mylonites. Passchier *et al.* (1993) proposed a model in which δ-type mantled porphyroclasts without stair-stepping are produced when the rheology of the matrix material is Newtonian ($n = 1$), whereas those with stair-stepping are produced when the rheology is non-Newtonian ($n > 1$). As both types of porphyroclast exist in mylonites, the model actually implies that n is not constant but varies from deformation to deformation. Passchier (1994) extended the model to explain other types (σ-, ϕ- and θ-types) of mantled porphyroclasts. This model, however, has no basis in theory, because no rheological analysis of deformation of a non-Newtonian viscous material around a sphere has so far been performed, although that for a Newtonian viscous material was reported by Einstein (1956), Cox *et al.* (1968), Masuda & Ando (1988), Bjornerud (1989) and Gray & Busa (1994).

This paper analyses the deflection of a non-Newtonian simple shear flow around a rigid cylindrical body, presenting a theoretical basis for this third method of inferring the value of n. It briefly summarizes the general

---

*Present address: Geology Division, CTI Engineering Co., Ltd, Nihonbashi Honcho, Tokyo 103, Japan.

three-dimensional equations for non-Newtonian flow and develops the solution of the two-dimensional equations using the Finite Element Method (FEM). The paper presents results on velocity vectors, particle paths and kinematic and dynamic quantities of the flow and shows how the magnitude of n influences these. Unfortunately, however, the results are not consistent with the model of Passchier *et al.* (1993) and Passchier (1994).

BASIC EQUATIONS

We consider the velocity of a fluid particle (u, v, w) in the Cartesian coordinate system (x, y, z). Since deformation within the Earth is very slow, the material is regarded as incompressible, and no acceleration and no body forces are assumed.

The equations of motion (e.g. Lamb 1932) are reduced to simple form as:

$$\frac{\partial \sigma_{xx}}{\partial x} + \frac{\partial \sigma_{xy}}{\partial y} + \frac{\partial \sigma_{xz}}{\partial z} = 0$$

$$\frac{\partial \sigma_{yx}}{\partial x} + \frac{\partial \sigma_{yy}}{\partial y} + \frac{\partial \sigma_{yz}}{\partial z} = 0 \qquad (1)$$

$$\frac{\partial \sigma_{zx}}{\partial x} + \frac{\partial \sigma_{zy}}{\partial y} + \frac{\partial \sigma_{zz}}{\partial z} = 0$$

where σ_{xx}, σ_{yy}, σ_{zz}, σ_{xy}, σ_{yx} ($= \sigma_{xy}$), σ_{yz}, σ_{zy} ($= \sigma_{yz}$), σ_{zx} and σ_{xz} ($= \sigma_{zx}$) are components of the stress tensor. The equation of continuity is

$$\frac{\partial u}{\partial x} + \frac{\partial v}{\partial y} + \frac{\partial w}{\partial z} = 0. \qquad (2)$$

The rheological equations for a power-law viscous fluid (Tomita 1975) give the relationship between stress and strain as

$$\sigma_{xx} = -p + 2K\Theta \dot{e}_{xx}$$

$$\sigma_{yy} = -p + 2K\Theta \dot{e}_{yy}$$

$$\sigma_{zz} = -p + 2K\Theta \dot{e}_{zz}$$

$$\sigma_{xy} = 2K\Theta \dot{e}_{xy} \qquad (3)$$

$$\sigma_{yz} = 2K\Theta \dot{e}_{yz}$$

$$\sigma_{zx} = 2K\Theta \dot{e}_{zx}$$

where p is the hydrostatic pressure, K is a constant. Θ is expressed as:

$$\Theta = [2\{\dot{e}_{xx}^2 + \dot{e}_{yy}^2 + \dot{e}_{zz}^2\} + 4\{\dot{e}_{xy}^2 + \dot{e}_{yz}^2 + \dot{e}_{zx}^2\}]^{(\frac{1}{n}-1)/2} \qquad (4)$$

where n is the stress exponent, and $\dot{e}_{xx}$, $\dot{e}_{yy}$, $\dot{e}_{zz}$, $\dot{e}_{xy}$, $\dot{e}_{yz}$ and $\dot{e}_{zx}$, are components of rate-of-strain tensor defined by

$$\dot{e}_{xx} = \frac{\partial u}{\partial x}$$

$$\dot{e}_{yy} = \frac{\partial v}{\partial y}$$

$$\dot{e}_{zz} = \frac{\partial w}{\partial z}$$

$$\dot{e}_{xy} = \frac{1}{2}\left(\frac{\partial v}{\partial x} + \frac{\partial u}{\partial y}\right) \qquad (5)$$

$$\dot{e}_{yz} = \frac{1}{2}\left(\frac{\partial w}{\partial y} + \frac{\partial v}{\partial z}\right)$$

$$\dot{e}_{zx} = \frac{1}{2}\left(\frac{\partial u}{\partial z} + \frac{\partial w}{\partial x}\right).$$

By substituting equation (3) into (1) and using equation (2), we obtain

$$K\Theta\nabla^2 u = \frac{\partial p}{\partial x} - K\left[2\frac{\partial \Theta}{\partial x}\frac{\partial u}{\partial x} + \frac{\partial \Theta}{\partial y}\left(\frac{\partial v}{\partial x} + \frac{\partial u}{\partial y}\right) + \frac{\partial \Theta}{\partial z}\left(\frac{\partial u}{\partial z} + \frac{\partial w}{\partial x}\right)\right]$$

$$K\Theta\nabla^2 v = \frac{\partial p}{\partial y} - K\left[2\frac{\partial \Theta}{\partial y}\frac{\partial v}{\partial y} + \frac{\partial \Theta}{\partial z}\left(\frac{\partial w}{\partial y} + \frac{\partial v}{\partial z}\right) + \frac{\partial \Theta}{\partial x}\left(\frac{\partial v}{\partial x} + \frac{\partial u}{\partial y}\right)\right]$$

$$K\Theta\nabla^2 w = \frac{\partial p}{\partial z} - K\left[2\frac{\partial \Theta}{\partial z}\frac{\partial w}{\partial z} + \frac{\partial \Theta}{\partial x}\left(\frac{\partial u}{\partial z} + \frac{\partial w}{\partial x}\right) + \frac{\partial \Theta}{\partial y}\left(\frac{\partial w}{\partial y} + \frac{\partial v}{\partial z}\right)\right] \qquad (6)$$

Equations (2) and (6) only concern variables u, v, w and p for a given n. If $n = 1$, $\Theta = 1$ in equation (4) and equations (6) are equivalent to the Navier–Stokes equations for very slow Newtonian viscous flow (e.g. Masuda & Ando 1988, equation 1). We wish to obtain values of u, v, w and p which satisfy these equations (2) and (6) in a restricted area surrounded by a closed periphery. Boundary conditions are given as constraints on the viscous flow along the periphery, and initial conditions are also required. If u, v, w and p are solved for stress and strain rate components can be derived from equations (3) and (5). However, it is difficult to solve equations (2) and (6) when $n \neq 1$.

FINITE ELEMENT METHOD

The variational principle (e.g. Tomita 1975, Bird *et al.* 1987) states that solving these partial differential equations (2) and (6) is equivalent to obtaining u, v, and w which give a stationary value (minimum in this case) for the functional J:

$$J = \frac{1}{\frac{1}{n}+1}\int\int\int \Phi \, \mathrm{d}x\mathrm{d}y\mathrm{d}z \qquad (7)$$

where

$$\Phi = [2\{\dot{e}_{xx}^2 + \dot{e}_{yy}^2 + \dot{e}_{zz}^2\} + 4\{\dot{e}_{xy}^2 + \dot{e}_{yz}^2 + \dot{e}_{zx}^2\}]^{(\frac{1}{n}+1)/2}$$
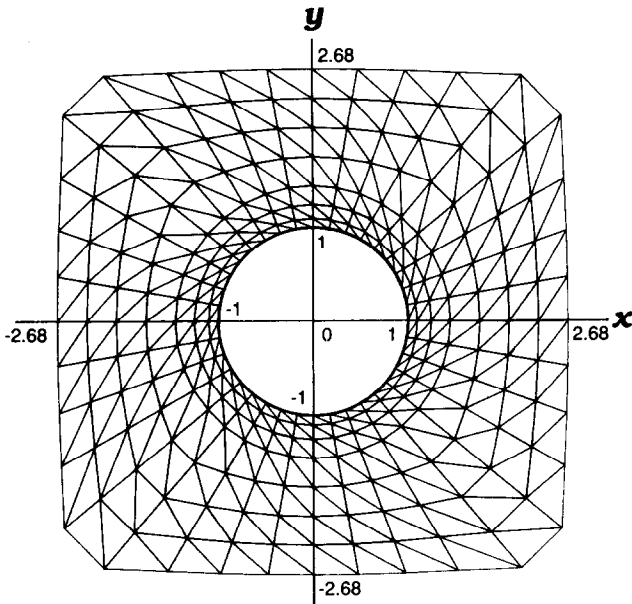
Fig. 1. Finite element grid used in the study, with 288 nodes and 504 triangular elements. Velocities (u, v) at 36 nodes on the periphery and 36 nodes on the central cylinder are given in accordance with the boundary conditions of the flow.

Φ is the dissipation function for the flow (e.g. Tomita 1975). We deal with equation (7) using the Finite Element Method (FEM).

For simplicity we analyse how the simple shear flow deflects around a rigid cylindrical body in two dimensions (x–y plane). The FEM analysis proceeds with the following steps.

(1) We define the study area (Fig. 1) and its boundary conditions on the x–y plane. The centre of the rigid cylindrical body is placed at the origin (0, 0). The radius of the rigid body is 1. No slip is assumed between the rigid body and the surrounding non-Newtonian viscous material. A time-independent flow is assumed in this system. Thus, we need no initial conditions for our analysis. The boundary conditions for u and v along the periphery of the area are given as

$$u = y \text{ and } v = 0,$$

representing a far-field dextral simple shear strain rate $(\dot{\gamma})$ of 1, and those around the rigid cylinder are

$$u = y\dot{\omega} \text{ and } v = -x\dot{\omega}$$

where $\dot{\omega}$ is the angular velocity of the rigid cylinder. For $\dot{\omega}$, we input 0.3–0.6. Determination of $\dot{\omega}$ will be performed later. As for n, we input 1, 2, 3, 4 and 5.

(2) In the study area, we set 288 nodes (Fig. 1). The area was then divided into 504 triangular elements with 3 nodes as vertices. The velocity (u, v) at 36 nodes on the periphery of the area and those at 36 nodes on the periphery of the central cylinder are given in accordance with the boundary conditions. The velocities at the remaining 216 nodes are unknown and to be solved. The known x–y coordinates and the unknown velocity at

ith node are termed (x_i, y_i) and (u_i, v_i) ($i = 1$–216), respectively.

(3) In each triangular element, u and v are assumed to be expressed as:

$$u = a + bx + cy$$

$$v = d + ex + fy \tag{8}$$

where a, b, c, d, e and f are unique constants for each triangular element.

(4) Consider a single triangular element whose vertices are i, j and kth nodes (Fig. 2a). Since velocity is (u_i, v_i) at (x_i, y_i), (u_j, v_j) at (x_j, y_j) and (u_k, v_k) at (x_k, y_k), the following equations are derived (e.g. Zienkiewicz 1977):

$$\begin{pmatrix} a \\ b \\ c \end{pmatrix} = \frac{1}{\Delta} \begin{pmatrix} x_j y_k - x_k y_j & x_k y_i - x_i y_k & x_i y_j - x_j y_i \\ y_j - y_k & y_k - y_i & y_i - y_j \\ x_k - x_j & x_i - x_k & x_j - x_i \end{pmatrix} \begin{pmatrix} u_i \\ u_j \\ u_k \end{pmatrix}$$

$$\begin{pmatrix} d \\ e \\ f \end{pmatrix} = \frac{1}{\Delta} \begin{pmatrix} x_j y_k - x_k y_i & x_k y_i - x_i y_k & x_i y_j - x_j y_i \\ y_j - y_k & y_k - y_i & y_i - y_j \\ x_k - x_j & x_i - x_k & x_j - x_i \end{pmatrix} \begin{pmatrix} v_i \\ v_j \\ v_k \end{pmatrix}$$

$$\tag{9}$$

where

$$\Delta = \begin{vmatrix} 1 & x_i & y_i \\ 1 & x_j & y_j \\ 1 & x_k & y_k \end{vmatrix}.$$

Since $\dot{e}_{xx}$, $\dot{e}_{yy}$ and $\dot{e}_{xy}$ are directly calculated from equation (8) as

$$\dot{e}_{xx} = \frac{\partial u}{\partial x} = b$$

$$\dot{e}_{yy} = \frac{\partial v}{\partial y} = f \tag{10}$$

$$\dot{e}_{xy} = \frac{1}{2}\left(\frac{\partial v}{\partial x} + \frac{\partial u}{\partial y}\right) = \frac{1}{2}(c + e)$$

and $\dot{e}_{zz} = \dot{e}_{yz} = \dot{e}_{zx} = 0$ (because we analyse on the x–y plane), Φ in the triangular element is reduced to

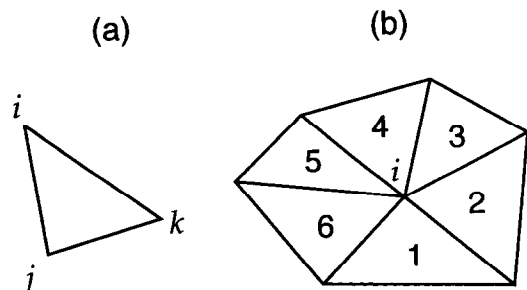$$\Phi = (2b^2 + 2f^2 + c^2 + 2ce + e^2)^{(\frac{1}{n}+1)/2}. \tag{11}$$

(a) (b)

Fig. 2. Schematic diagram of triangular elements for the FEM. (a) Unit triangular element whose node numbers are i, j and k. (b) Six triangular elements around ith node.

Then, J for the triangular element can be expressed as

$$J = \frac{1}{\frac{1}{n}+1} \int\int \Phi dx dy$$

$$= \frac{1}{\frac{1}{n}+1} \int\int (2b^2 + 2f^2 + c^2 + 2ce + e^2)^{(\frac{1}{n}+1)/2} dx dy$$

$$= \frac{1}{\frac{1}{n}+1} (2b^2 + 2f^2 + c^2 + 2ce + e^2)^{(\frac{1}{n}+1)/2} \int\int dx dy. \tag{12}$$

As

$$\frac{\Delta}{2} = \int\int dx dy, \tag{13}$$

equation (12) eventually is reduced to

$$J = \frac{1}{\frac{1}{n}+1} \frac{\Delta}{2} (2b^2 + 2f^2 + c^2 + 2ce + e^2)^{(\frac{1}{n}-1)/2}. \tag{14}$$

Thus, J for the triangular element is given as a function of six unknown variables (u_i, v_i, u_j, v_j, u_k and v_k).

(5) In the same way, we expand the integration of J for other triangular elements, and consequently cover all the study area. Then, J can be expressed as a polynomial function of u_i and v_i ($i = 1–216$). Since J is required to have a stationary value by the variational principle, the following 432 equations should be simultaneously satisfied:

$$\frac{\partial J}{\partial u_i} = 0$$

$$\frac{\partial J}{\partial v_i} = 0.$$

$$(i = 1 \text{ to } 216) \tag{15}$$

All u and v at 216 nodes are unknown variables of a system of 432 equations. Our problem, to know how simple shear flow deflects around the rigid cylindrical body, is consequently replaced by the problem of obtaining u_i and v_i ($i = 1$ to 216) by solving equation (15).

(6) Practically, we separately formulated $\partial J/\partial u_i = 0$ and $\partial J/\partial v_i = 0$ for each i. The ith node is a vertex of six triangular elements (Fig. 2b), and u_i and v_i only appear in the integration of J for the six triangular elements. Thus, by numbering the triangular elements around ith node from 1 to 6 (Fig. 2b),

$$\frac{\partial J}{\partial u_i} = \sum_{m=1}^{6} \frac{\partial J_m}{\partial u_i} = \frac{\partial J_1}{\partial u_i} + \frac{\partial J_2}{\partial u_i} + \frac{\partial J_3}{\partial u_i} + \frac{\partial J_4}{\partial u_i} + \frac{\partial J_5}{\partial u_i} + \frac{\partial J_6}{\partial u_i}$$

$$\frac{\partial J}{\partial v_i} = \sum_{m=1}^{6} \frac{\partial J_m}{\partial v_i} = \frac{\partial J_1}{\partial v_i} + \frac{\partial J_2}{\partial v_i} + \frac{\partial J_3}{\partial v_i} + \frac{\partial J_4}{\partial v_i} + \frac{\partial J_5}{\partial v_i} + \frac{\partial J_6}{\partial v_i} \tag{16}$$

where J_m ($m = 1–6$) is J for the mth triangular element. We concentrate our calculation on one (mth) triangular element among the six. From equation (14),

$$J_m = \frac{1}{\frac{1}{n}+1} \frac{\Delta_m}{2} (2b_m^2 + 2f_m^2 + c_m^2 + 2c_m e_m + e_m^2)^{(\frac{1}{n}+1)/2} \tag{17}$$

where Δ_m, b_m, f_m, c_m, e_m are values of Δ, b, f, c and e, respectively, calculated from equation (9) for the mth triangular element. Thus,

$$\frac{\partial J_m}{\partial u_i} = \frac{1}{\frac{1}{n}+1} \frac{\Delta_m}{2} \frac{\frac{1}{n}+1}{2}$$

$$\times (2b_m^2 + 2f_m^2 + c_m^2 + 2c_m e_m + e_m^2)^{(\frac{1}{n}-1)/2}$$

$$\times \left(4b_m \frac{\partial b_m}{\partial u_i} + 4f_m \frac{\partial f_m}{\partial u_i} + 2c_m \frac{\partial c_m}{\partial u_i} + 2c_m \frac{\partial e_m}{\partial u_i} \right.$$

$$\left. + 2e_m \frac{\partial c_m}{\partial u_i} + 2e_m \frac{\partial e_m}{\partial u_i} \right). \tag{18}$$

In this equation,

$$\frac{\partial f_m}{\partial u_i} = \frac{\partial e_m}{\partial u_i} = 0,$$

$$\frac{\partial b_m}{\partial u_i} = \frac{y_j - y_k}{\Delta_m}, \tag{19}$$

$$\frac{\partial c_m}{\partial u_i} = \frac{x_k - x_j}{\Delta_m},$$

which leads to

$$\frac{\partial J_m}{\partial u_i} = \frac{1}{4} (2b_m^2 + 2f_m^2 + c_m^2 + 2c_m e_m + e_m^2)^{(\frac{1}{n}-1)/2}$$

$$[4b_m(y_j - y_k) + 2c_m(x_k - x_j) + 2e_m(x_k - x_j)] \tag{20}$$

where x_j, x_k and y_j, y_k are the x and y coordinates of the other two nodes (j and kth nodes) of the mth triangular element, respectively. Similarly,

$$\frac{\partial J_m}{\partial v_i} = \frac{1}{4} (2b_m^2 + 2f_m^2 + c_m^2 + 2c_m e_m + e_m^2)^{(\frac{1}{n}-1)/2}$$

$$[4f_m(x_k - x_j) + 2c_m(y_j - y_k) + 2e_m(y_j - y_k)] \tag{21}$$

was derived. Expanding the similar calculation to the other five triangular elements,

$$\frac{\partial J}{\partial u_i} = \sum_{m=1}^{6} \frac{\partial J_m}{\partial u_i} = 0$$

$$\frac{\partial J}{\partial v_i} = \sum_{m=1}^{6} \frac{\partial J_m}{\partial v_i} = 0 \tag{22}$$

are derived as non-linear multiple-variable equations. As the six triangular elements around ith node contain the other six nodes, u and v at a total of seven nodes are the variables of equation (22). Thus, each equation of (22) has 14 unknown variables.

(7) The system of non-linear equations (22) for $i = 1–216$, was solved with Newton's method (e.g. Ortega &

Rheinboldt 1970) using a UNIX computer at Shizuoka University.

(8) Since there is no theory giving the angular velocity ($\dot\omega$) of a rigid cylinder embedded in a simple-shear flow of a non-Newtonian viscous matrix (cf. Jeffery 1922), we must determine $\dot\omega$. Since u and v are dependent on the given value of $\dot\omega$ in the calculation, we introduce a new constraint for the determination of $\dot\omega$: i.e. total rotational moment of the rigid cylinder (M). From the u and v obtained for different $\dot\omega$, we calculate M around the cylinder in a polar coordinate system (r, θ) as

$$M = \int_0^{2\pi} r\tau_{r\theta}\mathrm{d}\theta \tag{23}$$

where

$$\tau_{r\theta} = K\Theta\left(\frac{1}{r}\frac{\partial V_r}{\partial\theta} - \frac{V_\theta}{r} + \frac{\partial V_\theta}{\partial r}\right),$$

$$\Theta = \left[2\left\{\left(\frac{\partial V_r}{\partial r}\right)^2 + \left(\frac{1}{r}\frac{\partial V_\theta}{\partial\theta} + \frac{V_r}{r}\right)^2\right\}\right.$$
$$\left. + \left(\frac{1}{r}\frac{\partial V_r}{\partial\theta} - \frac{V_\theta}{r} + \frac{\partial V_\theta}{\partial r}\right)^2\right]^{(\frac{1}{n}-1)/2}$$

K is the constant in equation (3), V_r are velocities parallel to the radial and circular axes, respectively, and $\tau_{r\theta}$ is tangential stress (e.g. Tomita 1975, Masuda et al. 1995). In this case $r = 1$. If $M > 0$, rotation of the cylinder will accelerate; if $M < 0$, decelerate; if $M = 0$, the cylinder will rotate at a constant angular velocity. The values of u and v for which we are searching should satisfy $M = 0$, because the flow is time-independent. We calculated M at different $\dot\omega$ ($\dot\omega = 0.30$, 0.40, 0.49, 0.50, 0.51, and 0.60) (Fig. 3) and found that the value of $\dot\omega = 0.50$ meets the requirement $M = 0$. This value of $\dot\omega$ indicates that the relationship between angular velocity ($\dot\omega$) and far-field simple shear strain rate ($\dot\gamma$) is expressed by

$$\dot\omega = \dot\gamma/2, \tag{24}$$

because we assumed $\dot\gamma = 1$. The relationship is exactly the same as that theoretically established by Jeffery (1922) for Newtonian viscous materials ($n = 1$), and is consistent with Ferguson (1979).

(9) To evaluate our FEM analysis, we compare the velocity vectors and particle paths obtained by the FEM for $n = 1$ (Fig. 4) with those calculated by analytical methods (Cox et al. 1968). The results of the two methods appear very similar. To quantify the difference, we compared the closed particle paths shown in Fig. 4(b).
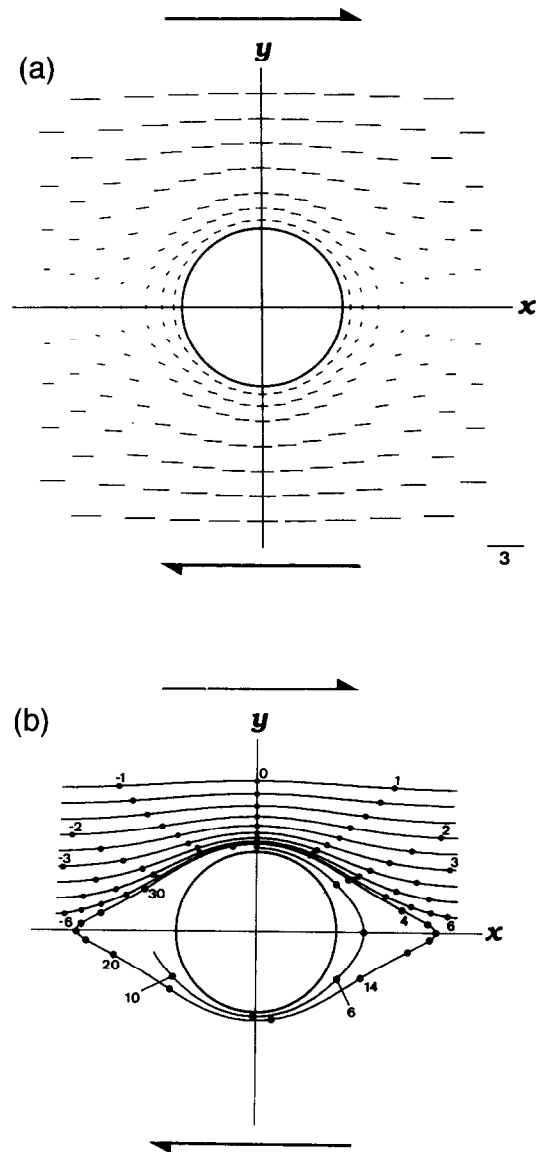
Fig. 4. Newtonian flow ($n = 1$) by FEM. (a) Velocity vector field. Scale bar at the right bottom corner. (b) Particle paths. Numbers attached to the points show far-field simple shear strain (γ) taken for the particle initially placed on the y axis ($y > 0$). The limiting closed and open paths are shown, which have $\rho_{min} = 1.10$, $\rho_{max} = 2.25$ and $\rho_{min} = 1.11$, $\rho_{max} = \infty$, respectively. (a) and (b) are very similar to figures obtained by analytical methods around a sphere (figs. 2 and 4 of Masuda & Ando 1988).
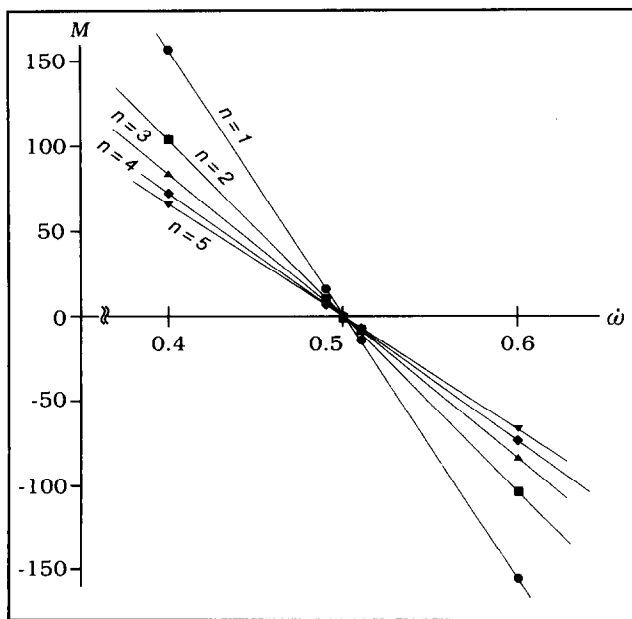
Fig. 3. Determination of $\dot\omega$ by the moment analysis. The moment M becomes zero when $\dot\omega$ is 0.50 for $n = 1$–5. The calculation of M was done assuming $K = 1$, which has no influence on the determination of $\dot\omega$. See text for explanation.

We denote the distance of the farthest and the nearest points of the particle path from the centre of the cylinder as ρ_{max} and ρ_{min}, which lie on the x and y axes, respectively. The outer particle path in Fig. 4 has ρ_{max} = 2.25 and ρ_{min} = 1.11 and the inner one ρ_{max} = 1.35 and ρ_{min} = 1.06, whereas the theoretical path with ρ_{max} = 2.25 shows ρ_{min} = 1.26 and that with ρ_{max} = 1.35 shows ρ_{min} = 1.16. Thus, our ρ_{min} understates the theoretical value by 12% and 9%, respectively. These values indicates that our FEM analysis gives a good (but not excellent) approximation to Newtonian flow, showing that the 288 nodes in our analysis are satisfactory. The number of nodes therefore should be satisfactory for $n > 1$ and the results shown below are presumably reliable, as a first approximation, although we cannot estimate by how many percent the FEM analysis under-values or overvalues quantities for actual non-Newtonian flows.

RESULTS

The results of our calculation on kinematic and dynamic quantities are presented below, focusing on how they are influenced by the magnitude of n. In general, the results for non-Newtonian viscous flows at different n are similar to those for Newtonian flow.

Velocity vector

Our FEM analysis at ω = 0.5 first gave the velocity vector at each node (Fig. 5). The flow is highly deflected by the presence of the cylinder. If we do not consider the direction of flow, the orientation and magnitude of velocity vectors are symmetric with the x and y axes. The pattern of the velocity vectors does not essentially change with increasing n (compare Fig. 5 with Fig. 4).

Particle paths

We apply the particle-path technique that was employed by Masuda & Ando (1988). Particle paths for n = 3 and 5 are shown in Fig. 6. Both particle paths are essentially similar. Each particle has a symmetrical path with respect to the x and y axes. Particles close to the cylinder exhibit ovoid orbits around the cylinder, whereas others have paths running away from the cylinder.

Separatrix

The separatrix is defined by the boundary surface between closed, ovoid paths around the cylinder and open paths moving away from the cylinder (Passchier et al. 1993, Passchier 1994). The classification of flow perturbations around a rigid body in terms of the type of separatrix ('eye shaped' and 'bow-tie shaped') was regarded as important by Passchier et al. (1993) and Passchier (1994). Consequently, we show in some depth how we determined the type and shape of the
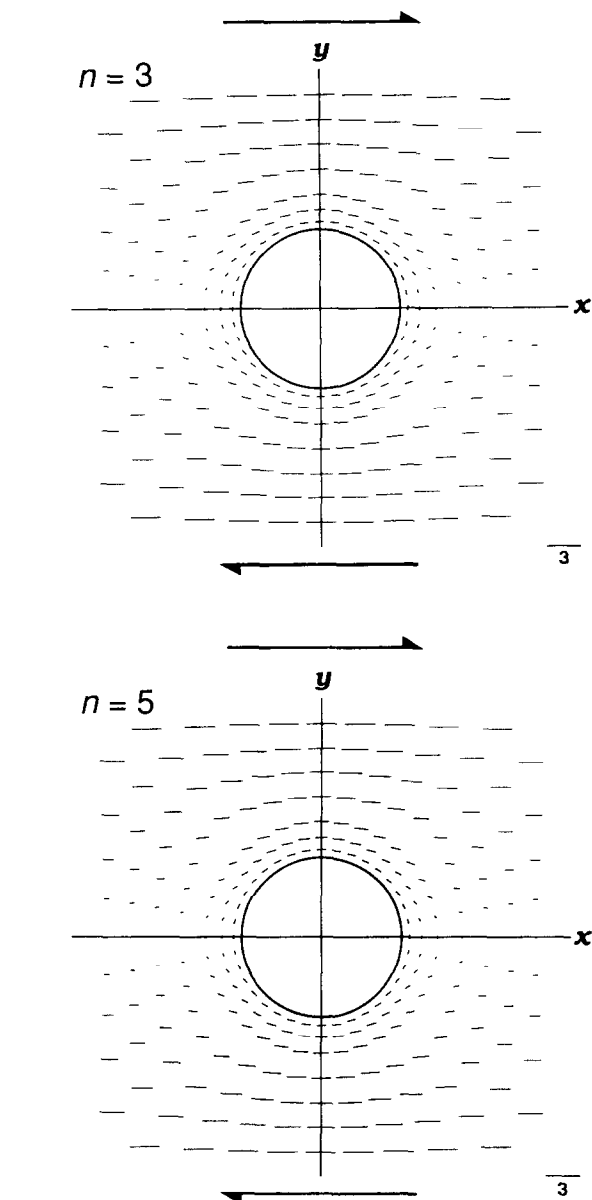

Fig. 5. Velocity vector fields for n = 3 and n = 5. Note close similarity to each other and also to Fig. 4(a) for n = 1. Scale bar in the right bottom corner.

separatrix for non-Newtonian simple shear flows as follows.

(1) Cox et al. (1968) studied theoretically the shape of the separatrix around a cylinder for a Newtonian flow, and concluded that the separatrix is 'double-bulge shaped' (Fig. 7) and that ρ_{max} = ∞ and ρ_{min} = 1.30656 for the separatrix (for ρ_{min} and ρ_{max} see (9) of the previous section). The latter result means that the separatrix surface converges on the x axis when $x \to \infty$. These conclusions are helpful when we consider the separatrix for non-Newtonian flows.

(2) We have no stagnation point (see Passchier et al. 1993, Passchier 1994) on the x axis in the limited analysed area. It is difficult to judge the type of separatrix by tracing the particle paths in the area shown in Fig. 1.
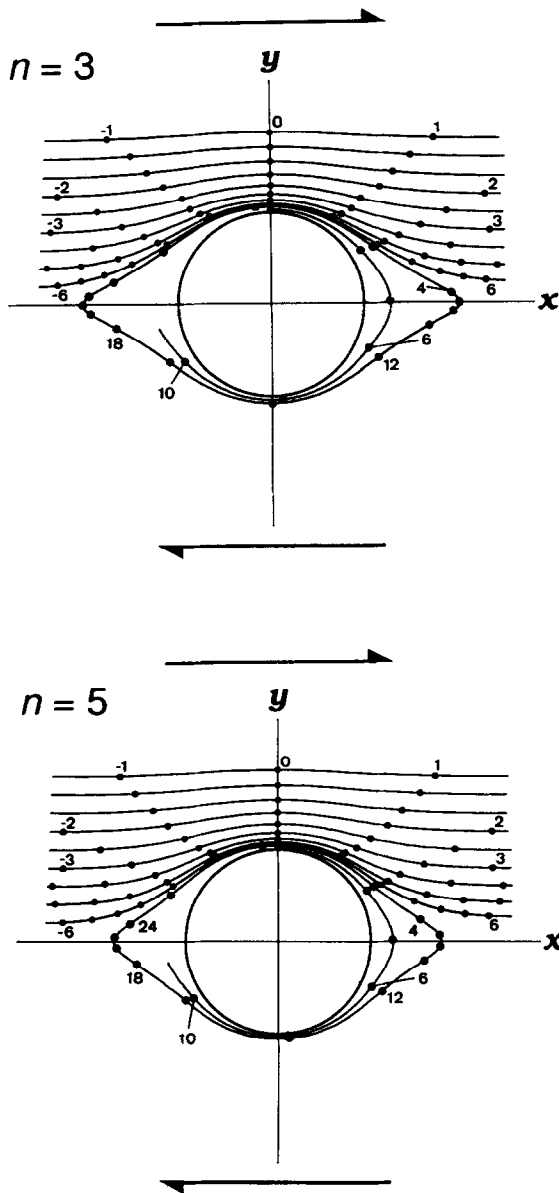
n = 3

n = 5

Fig. 6. Particle paths for $n = 3$ and $n = 5$. Note similarity to each other and also to Fig. 4(b) for $n = 1$. Numbers attached to the points show far-field simple shear strain (γ) taken for the particle initially placed on the y axis ($y > 0$). The limiting closed and open paths are shown, which have $\rho_{min} = 1.07$, $\rho_{max} = 2.03$ and $\rho_{min} = 1.08$, $\rho_{max} = \infty$, respectively, for $n = 3$, and $\rho_{min} = 1.05$, $\rho_{max} = 1.77$ and $\rho_{min} = 1.06$, $\rho_{max} = \infty$, respectively, for $n = 5$.

(3) In order to know what happens outside the area, we derived velocity vectors there as

$$u = \dot{\gamma}y + 0.5\dot{\gamma}y(x^2 + y^2)^{-(2n+1)/2}$$
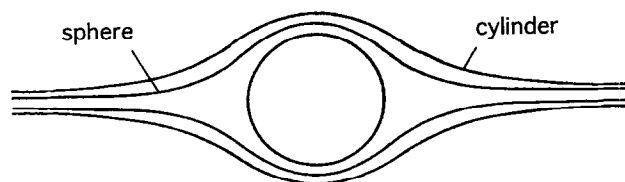$$v = -0.5\dot{\gamma}x(x^2 + y^2)^{-(2n+1)/2}. \qquad (25)$$

Fig. 7. The shape of separatrix around a cylinder for Newtonian matrix ($n = 1$) after Cox et al. (1968). The separatrix is double-bulge shaped. This figure also shows the separatrix around a sphere, which is similar to but smaller than that around a cylinder.

The way we derived them is explained in the Appendix.

(4) The velocity vectors (25) show that $v < 0$ when $x > 0$, $y > 0$. This indicates that no stagnation point exists on the x axis for the separatrix, because existence of the stagnation point requires $v > 0$ at $x > 0$, $y > 0$ ($y \sim 0$). It indicates $\rho_{max} = \infty$ for the separatrix. Thus, non-Newtonian flows have 'double-bulge shaped' separatrices like those for Newtonian flows (Fig. 7).

(5) We wish to determine ρ_{min} of the separatrix. From equation (25), we cannot obtain analytically the x and y coordinates of the separatrix. We judged whether the path is open or closed by tracing the particle originating at $(0, \rho_{min})$ up to $x = 10$: if $z > 0$ at $x = 10$, the path was judged open; if $z \leq 0$ at $x = 10$, the path was considered closed. Giving ρ_{min} iteratively, we searched ρ_{min} for the separatrix.

(6) The value of ρ_{min} of the separatrix should be between 1.10 and 1.11, 1.07 and 1.08, and 1.05 and 1.06 for $n = 1$, 3 and 5, respectively. ρ_{min} of the separatrix slightly decreases with increasing n. The limiting paths having $\rho_{min} = 1.10$ (closed path) and 1.11 (open) for $n = 1$, $\rho_{min} = 1.07$ (closed) and 1.08 (open) for $n = 3$, and $\rho_{min} = 1.05$ (closed) and 1.06 (open) for $n = 5$ are shown in Fig. 4(b) and 6.

Distortion of lines and determination of strain ellipses

Distortion of lines can be depicted by tracing a number of points initially arranged in a line using the particle-path technique. The patterns of distorted lines for $n = 1$–5 are similar. Figure 8 shows the pattern for $n = 5$. These appear similar to those around a sphere for $n = 1$ (fig. 5 of Masuda & Ando 1988).

Similarly strain ellipses can be obtained by tracing points initially arranged in a circle (Fig. 9). The elongation directions of the strain ellipses are similar for $n = 3$ and 5, wrapping around the cylinder. The patterns are also similar to those around a sphere for $n = 1$ (fig. 6 of Masuda & Ando 1988).

Principal stresses

Components of the stress tensor (σ_{xx}, σ_{yy} and σ_{xy}) are derived from equation (3) and used to calculate the magnitudes of the principal stresses (σ_1 and σ_2) and their orientations (Jaeger & Cook 1969). In order to remove the influence of a non-Newtonian material constant (K) from the magnitude of stress, we show normalised stress (stress/K) which is independent of the value of K. Figure 10 shows the magnitudes and orientations of σ_1/K and σ_2/K for $n = 5$. They are similar to those for $n = 1$–4.

Pressure

Pressure p is calculated as:

$$p = \frac{1}{2}(\sigma_{xx} + \sigma_{yy}) = \frac{1}{2}K\Theta(\dot{e}_{xx} + \dot{e}_{yy}). \qquad (26)$$

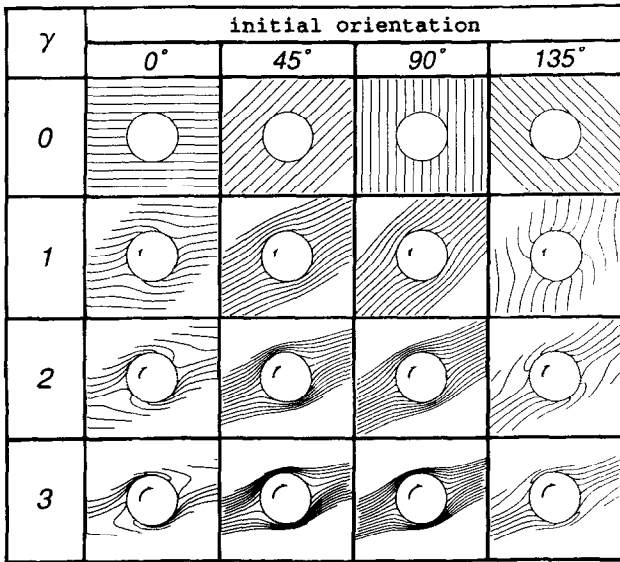In this calculation the far-field pressure is assumed to be zero. Figure 11(a) shows the distribution of p/K

Fig. 8. Distortion of lines for $n = 5$. These patterns are similar to those for a Newtonian flow around a rigid sphere shown in Masuda & Ando (1988). Patterns for $n = 1$–4 (not shown) are similar to those for $n = 5$. γ = far-field simple shear strain.

around the cylinder for $n = 3$ and 5. As $\dot{e}_{xx}$ and $\dot{e}_{yy}$ are constant in each triangular element, p is uniform in the element. The distribution has a 2-fold symmetric axis, and a 4-fold one if we do not consider the sign of the values. Pressure reaches a maximum and a minimum at half-way between the x and z axes, and the positions are the same for different n. The maximum value of p/K is 0.41, 0.36 and 0.35 for $n = 1$, 3 and 5, respectively. These magnitudes become slightly smaller as n increases (Fig. 11).

Differential stress

Figure 11(b) shows the magnitude of normalized differential stress $(\sigma_1 - \sigma_2)/K$. Differential stress reaches a maximum on the x and y axes around the cylinder, whereas its minimum values are half-way between these axes. The magnitude of differential stress becomes smaller with increasing n in areas close to the cylinder, whereas it remains constant for different n in areas far from the cylinder. The maximum differential stress is 2.84, 2.46 and 2.34 for $n = 1$, 3 and 5, respectively. Stress
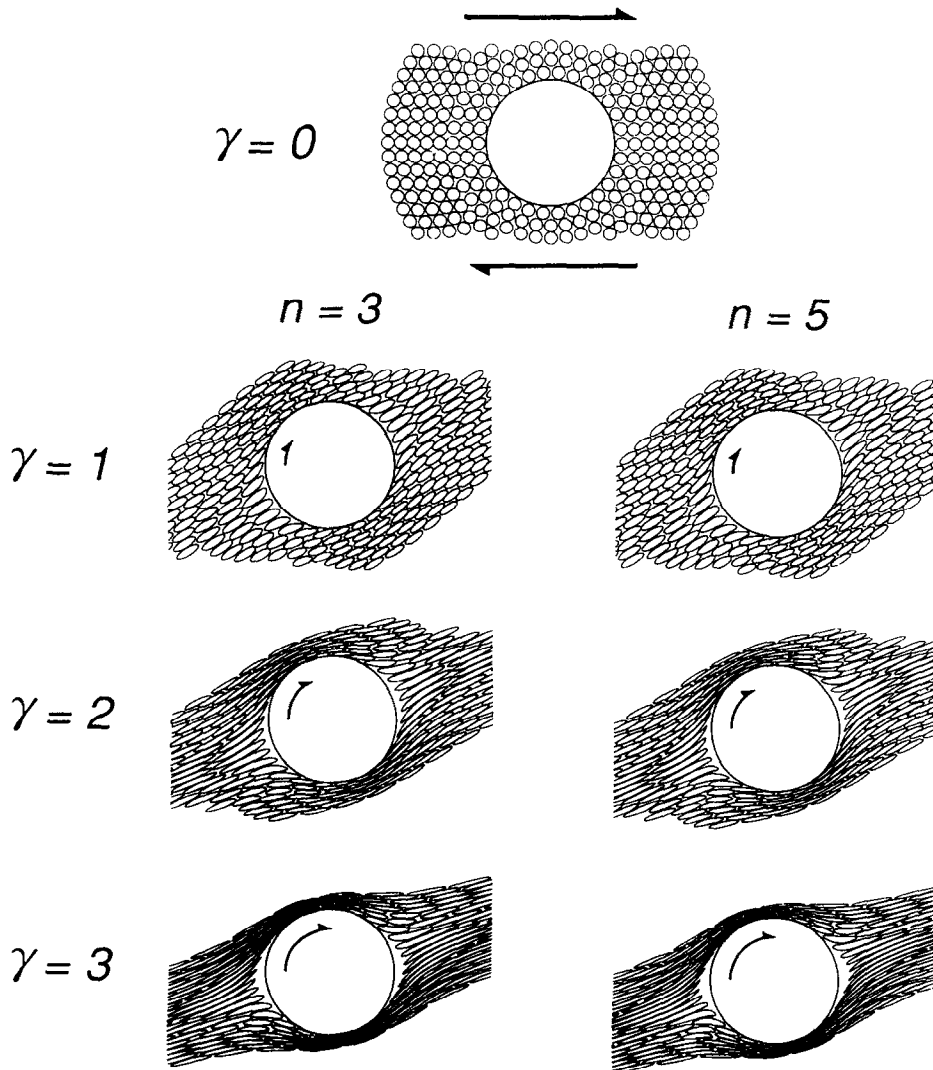

Fig. 9. Strain ellipses for $n = 3$ and $n = 5$ as a function of far-field simple shear strain γ. They are similar at the same γ.
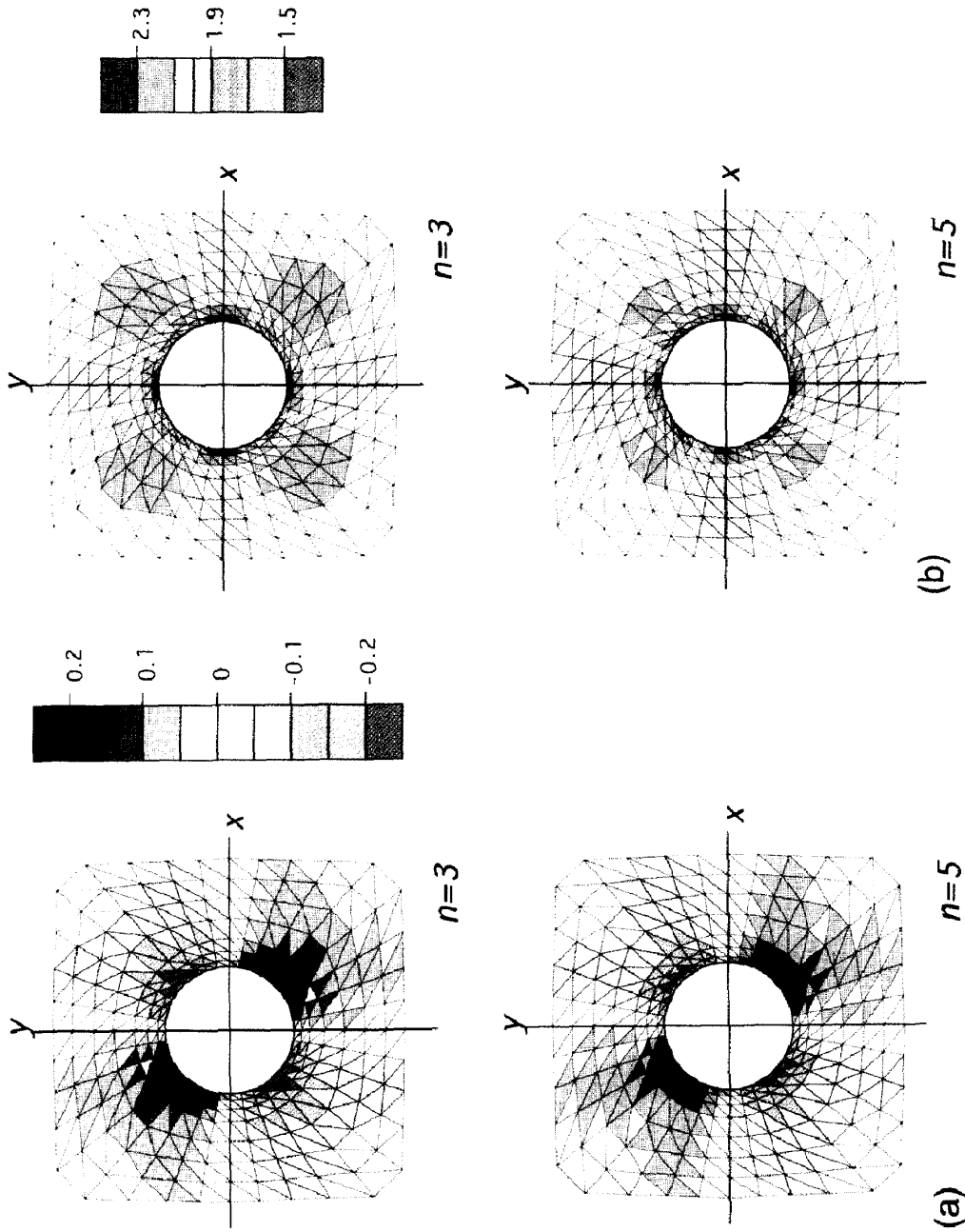
Fig. 11. (a) Magnitude of pressure/K [s^{-1}] for $n = 3$ and 5. Compression is taken positive. The far-field value is zero. The intensification of p/K around the cylinder slightly decreases with increasing n. (b) Magnitude of differential stress/K [s^{-1}] for $n = 3$ and 5. The far-field value is 2. The intensification of differential stress slightly decreases with increasing n.
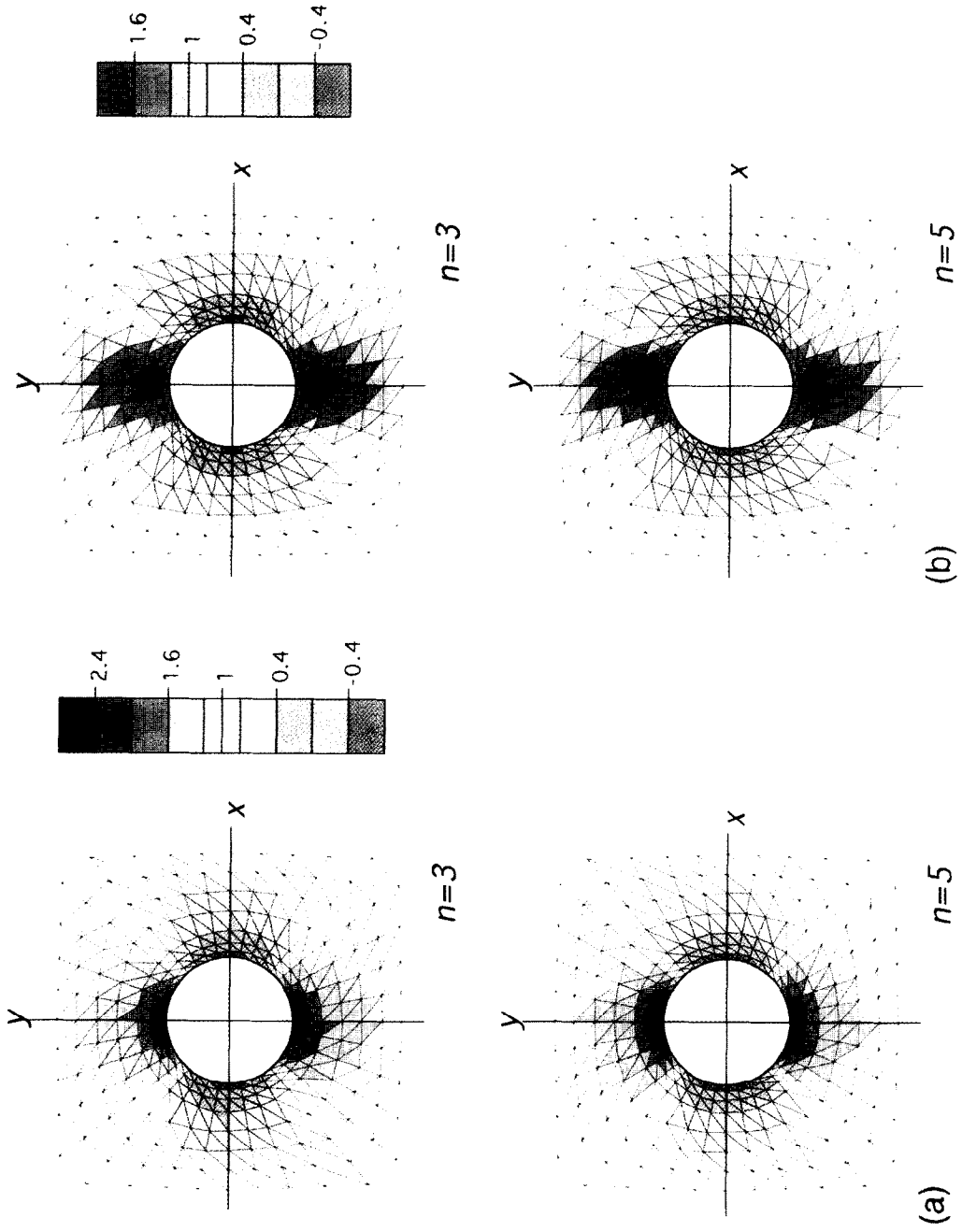
Fig. 12. (a) Magnitude of vorticity [s^{-1}] for $n = 3$ and 5. The far-field value is 1. The intensity of perturbation of vorticity becomes slightly larger at larger n, although perturbed region and general pattern of distribution seems independent of the value of n. (b) Kinematic vorticity number for $n = 3$ and 5. The far-field value is 1. The two distributions are very similar.
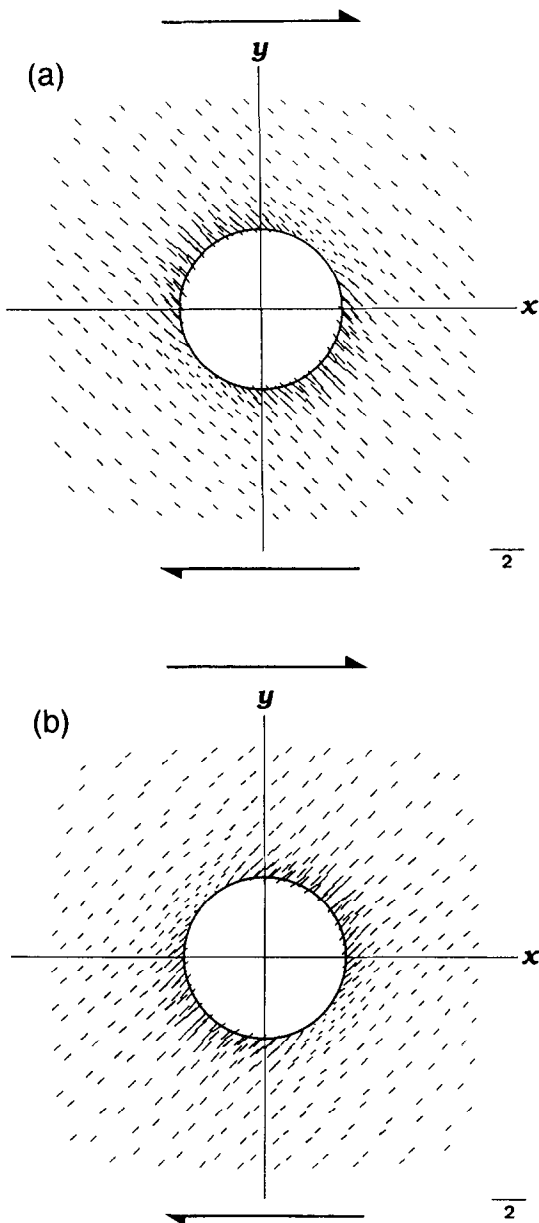
Fig. 10. Principal orientations of rate-of-strain tensor [s^{-1}] for $n = 5$. Extensional principal strain rates are shown in (a) and compressional ones in (b). Those for $n = 1$–4 (not shown) are very similar to them.

intensification due to the existence of a cylinder slightly weakens with increasing n.

Vorticity

Vorticity (ω_v) is defined by $\omega_v = \partial u/\partial y - \partial v/\partial x$. This definition indicates positive vorticity for dextral shear. Figure 12(a) shows the variation in vorticity around the cylinder. Vorticity becomes negative in the small area close to the cylinder on the x axis where shear sense is sinistral. The general pattern of distribution appears unchanged with increasing n. The maximum value of ω_v is 2.40, 2.84 and 3.14 for $n = 1$, 3 and 5, respectively, and dissipates to the far-field value ($\omega_v = 1$) slightly quicker for $n = 5$ than for $n = 1$.

Kinematic vorticity number

Figure 12(b) shows the kinematic vorticity number, W_k, defined by Means *et al.* (1980):

$$W_k = \frac{\omega_v}{\sqrt{2(s_1^2 + s_2^2 + s_3^2)}} \qquad (27)$$

where s_1, s_2 and s_3 are the principal strain rates. As with the vorticity, W_k is positive and negative when shear sense is dextral and sinistral, respectively. The far-field value is 1. The maximum value of W_k is 1.80, 1.82 and 1.83 for $n = 1$, 3 and 5, respectively, almost constant with increasing n.

DISCUSSION

Influence of the magnitude of n

Stress and strain analyses in two-dimensional annular shear zones (Masuda *et al.* 1995) revealed that differential stress and strain rates are highly influenced by the magnitude of n, resulting in very different distributions of strain ellipses as a function of n in the shear zones. The strain localization becomes more prominent with increasing n. Therefore, in the present analysis we expected a similar major influence of n on the velocity vector field, with deflection of marker lines and kinematic and dynamic quantities. However, as described above, the influence of n on these factors is small. This difference may be explained by considering the boundary conditions. In the annular shear zone, the angular velocity of the inner boundary is kept constant, whereas differential stress in the shear zone decreases with increase in the distance from the inner boundary. This decrease in stress value (τ) reflects the decrease in strain rate ($\dot{\gamma}$) with distance. Since $\dot{\gamma} \propto \tau^n$, n has a large influence on $\dot{\gamma}$.

We also considered a straight shear zone without any inclusions. If we assume a similar value of strain rate at the boundaries of the shear zone as the boundary condition of the equations (2) and (6), we can derive the same strain rate everywhere irrespective of n. In such a case, the shear stress τ is expressed as $\tau \propto \dot{\gamma}^{1/n}$. Thus, t should not be drastically influenced by n. The relationship we obtained between stress and strain rate around a cylinder is similar to the latter case.

CONCLUSIONS

(1) The Finite Element Method can be successfully applied to power-law, simple shear flows with $n = 1$–5 around a rigid cylinder.

(2) $\dot{\omega} = \dot{\gamma}/2$ for $n = 1$–5.

(3) Distributions of velocity vectors for $n = 1$–5 are similar.

(4) The separatrices are all 'double-bulge shaped'. The size of the separatrix slightly decreases with increasing n.

(5) Distribution patterns of kinematic and dynamic quantities are similar for $n = 1$–5 as a first approximation.

REFERENCES

Bird, R. B., Armstrong, R. C. & Hassager, O. 1987. *Dynamics of Polymer Liquids. Volume 1, Fluid Mechanics.* Wiley, New York.

Bjornerud, M. 1989. Mathematical model for folding of layering near rigid objects in shear deformation. *J. Struct. Geol.* **11**, 245–254.

Carter, N. L. & Tsenn, M. C. 1987. Flow properties of continental lithosphere. *Tectonophysics* **136**, 27–63.

Cox, R. G., Zia, Y. Z. & Mason, S. G. 1968. Particle motions in sheared suspensions. XXV. Streamlines around cylinders and spheres. *J. Colloid Interface Sci.* **27**, 7–18.

Einstein, A. 1956. *Investigations on the Theory of the Brownian Movement* (edited by Furth, R.). Dover, New York.

Ferguson, C. C. 1979. Rotation of elongate rigid particles in slow non-Newtonian flows. *Tectonophysics* **60**, 247–262.

Gray, N. H. & Busa, M. D. 1994. The three-dimensional geometry of simulated porphyroblast inclusion trails: inert-marker, viscous-flow models. *J. Metamorph. Geol.* **12**, 575–587.

Hudleston, P. J. & Lan, L. 1994. Rheological controls on the shapes of single-layer folds. *J. Struct. Geol.* **16**, 1007–1021.

Jaeger, J. C. & Cook, N. G. W. 1969. *Fundamentals of Rock Mechanics.* Chapman and Hall, London.

Jeffery, G. B. 1922. The motion of ellipsoidal particles immersed in a viscous fluid. *Proc. R. Soc. London, Ser. A* **102**, 161–179.

Kirby, S. H. & McCormick, J. W. 1989. Inelastic properties of rocks & minerals: strength and rheology. In: *Practical Handbook of Physical Properties of Rocks and Minerals* (edited by Carmichael, R. S.). Boca Raton, CRC Press, 177–297.

Lamb, H. 1932. *Hydrodynamics.* Cambridge University Press, Cambridge.

Masuda, T. & Ando, S. 1988. Viscous flow around a rigid spherical body: numerical simulation. *Tectonophysics* **148**, 337–346.

Masuda, T., Mizuno, N., Kobayashi, M., Nam, T. N. & Otoh, S. 1995. Stress and strain estimates for Newtonian and non-Newtonian materials in a rotational shear zone. *J. Struct. Geol.* **17**, 451–454.

Means, W. D., Hobbs, B. E., Lister, G. S. & Williams, P. F. 1980. Vorticity and non-coaxiality in progressive deformation. *J. Struct. Geol.* **2**, 371–378.

Nicolas, A. & Poirier, J. P. 1976. *Crystalline Plasticity and Solid State Flow in Metamorphic Rocks.* John Wiley and Sons, London.

Ortega J. M. & Rheinboldt, W. C. 1970. *Iterative Solution of Nonlinear Equations in Several Variables.* Academic Press, New York.

Passschier, C. W. 1994. Mixing in flow perturbations: a model for development of mantled porphyroclasts in mylonites. *J. Struct. Geol.* **16**, 733–736.

Passchier, C. W., Ten Brink, C. E., Bons, P. D. & Sokoutis, D. 1993. δ objects as a gauge for stress sensitivity of strain rate in mylonites. *Earth Planet. Sci. Lett.* **120**, 239–245.

Poirier, J. P. 1985. *Creep of Crystals.* Cambridge University Press, Cambridge.

Tomita, Y. 1975. *Rheology.* Corona Publishing, Tokyo (in Japanese).

Wang, J. N., Hobbs, B. E., Ord, A., Shimamoto, T. & Toriumi, M. 1994. Newtonian dislocation creep in quartzites: implications for the rheology of the lower crust. *Science, N.Y.* **265**, 1204–1206.

Zienkiewicz, O. C. 1977. *The Finite Element Method.* McGraw-Hill, London.

APPENDIX

The velocity vector is decomposed into two vectors: one related to the far-field simple shear flow and one influenced by the rotating cylinder. We consider (u, v) at a point (x, y) outside the analysed area (Fig. 1).

The component of (u, v) related to the far-field simple shear flow is given as

$$u = \dot{\gamma}y$$

$$v = 0. \tag{A1}$$

The influence of the rotating cylinder can be described by the angular velocity, $\dot{\theta}$, for an annular shear zone, which is given by e.g. Masuda *et al.* (1995) as

$$\dot{\theta} = \frac{\Omega_i - \Omega_e}{\frac{1}{R_i^{2n}} - \frac{1}{R_e^{2n}}} \frac{1}{r^{2n}} + \frac{R_i^{2n}\Omega_i - R_e^{2n}\Omega_e}{R_i^{2n} - R_e^{2n}} \tag{A2}$$

where r is the distance between the particle and the centre of the rotation, R_i and R_e are the radii of internal and external boundaries of the rotational shear zone, and Ω_i and Ω_e, the angular velocities at $r = R_i$ and $r = R_e$, respectively. In our case, we substitute $R_i = 1$, $R_e = \infty$, $\Theta_i = \dot{\gamma}/2$ and $\Omega_e = 0$, and obtain a simplified relationship between θ and r as

$$\dot{\Theta} = -0.5\dot{\gamma}r^{-2n}. \tag{A3}$$

This leads

$$u = -\dot{\theta}\sin\theta = 0.5\dot{\gamma}yr^{-2n-1} = 0.5\dot{\gamma}y(x^2 + y^2)^{-(2n+1)/2}$$

$$v = \dot{\theta}\cos\theta = -0.5\dot{\gamma}xr^{-2n-1} = -0.5\dot{\gamma}x(x^2 + y^2)^{-(2n+1)/2}. \tag{A4}$$

Adding far-field simple shear component (A1) and rotational component around the cylinder (A4), we obtain the approximate velocity vector outside the analysed area:

$$u = \dot{\gamma}y + 0.5\dot{\gamma}y(x^2 + y^2)^{-(2n+1)/2}$$

$$v = -0.5\dot{\gamma}x(x^2 + y^2)^{-(2n+1)/2}. \tag{A5}$$